Virtual Element Method for finite strain crystal plasticity

C. Böhm, B. Hudobivnik,
F. Aldakheel, P. Wriggers

Institute of Continuum Mechanics,
Leibniz Universität Hannover

Leibniz Universität Hannover

January 11 to 15, 2021

14th WCCM-ECCOMAS Congress
Minisymposium 378
Virtual Element Formulations for Engineering Applications

Contents

- Motivation
- Constitutive Framework
- Computational Approach: The Virtual Element Method
- Material Setup
- Representative numerical examples
- Conclusion
- Acknowledgement
- References

Motivation - Why VEM for crystalline Environments

- Crystalline environments are geometrically heterogeneous
- Require partially higher mesh refinements to maintain accuracy

⇒ Virtual Elements provide abilities to fit grain-geometries perfectly [2]

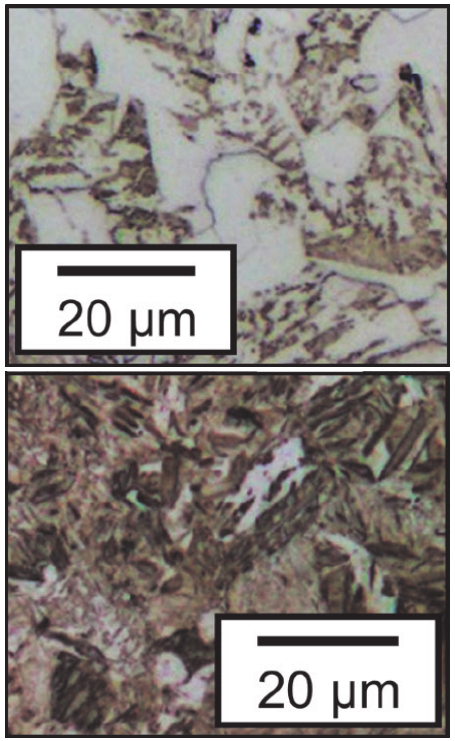

Fig. 1 Micrographs of induction-hardened steel-aluminum rods [1]

Constitutive Framework: Basics

Based on multiplicative split
$\mathbf{F} = \mathbf{F}_e \mathbf{F}_p$

$\rightarrow$ Internal variables are the plastic shears γ^α

$\Rightarrow$ Plasticity is solved at intermediate configuration $\mathcal{B}_e$

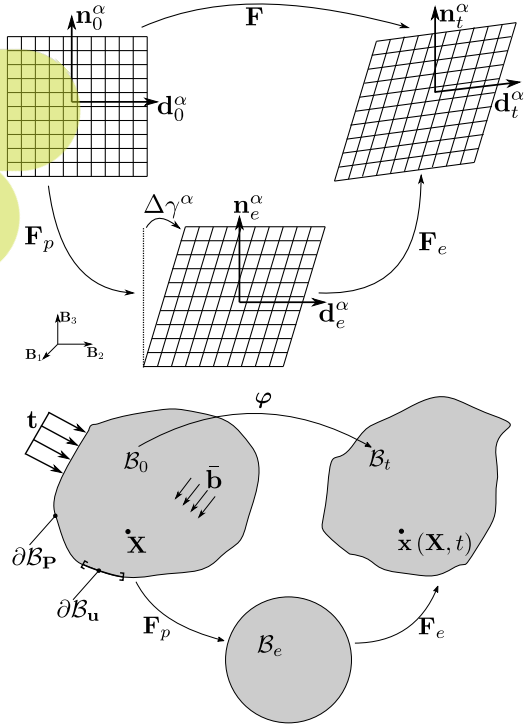

Fig. 2 Mapping of crystallographic system α by $\mathbf{F}_e$ and $\mathbf{F}_p$; Deformation map $\varphi : \mathcal{B}_0 \times T \rightarrow \mathcal{B}_t$

Constitutive Framework: Dissipation

Dissipation postulate in $\mathcal{B}_e$

$$\mathcal{D}^{red}_{loc} := \boldsymbol{\Sigma}_e : \mathbf{L}_p - \frac{\partial W(\mathbf{C}_e, \mathfrak{q})}{\partial \mathfrak{q}} \cdot \dot{\mathfrak{q}} \geq 0$$

- $\boldsymbol{\Sigma}_e$ - Mandel stress
- $\mathbf{L}_p$ - plastic part of gradient of velocity

Choice: $W = W(\mathbf{C}_e(\mathfrak{q})) = \frac{\mu}{2}(I_{e1} - 3) + \frac{\lambda}{4}(J_e^2 - 1) - (\frac{\lambda}{2} + \mu) log J_e$

$I_{e1} = \mathrm{Tr}[\mathbf{C}_e],\ J_e = \sqrt{\mathrm{Det}[\mathbf{C}_e]}$

$$\Rightarrow \mathcal{D}^{red}_{loc} = \boldsymbol{\Sigma}_e : \mathbf{L}_p \geq 0$$

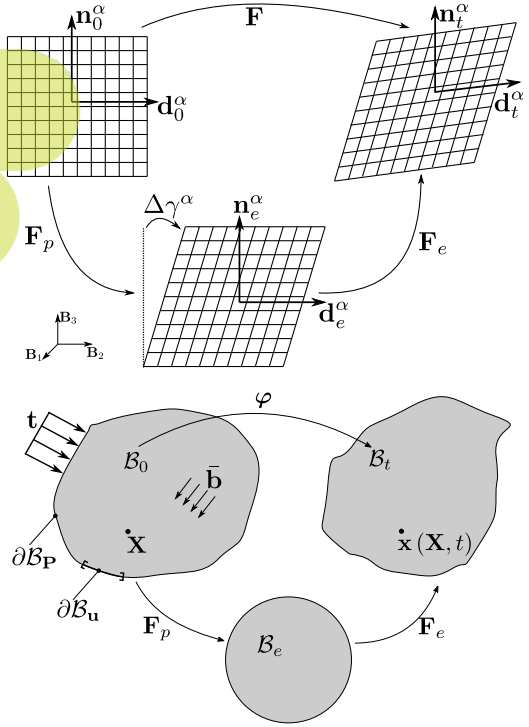

Fig. 2 Mapping of crystallographic system α by $\mathbf{F}_e$ and $\mathbf{F}_p$; Deformation map $\varphi : \mathcal{B}_0 \times T \to \mathcal{B}_t$

Constitutive Framework: Evolution Equations

Evolution equations:

$$\mathbf{L}_p = \dot{\mathbf{F}}_p \mathbf{F}_p^{-1} = \sum_\alpha \dot{\gamma}^\alpha \mathbf{m}^\alpha$$

$$\frac{\mathrm{d}}{\mathrm{dt}}\gamma^\alpha = \mathrm{sign}(\tau^\alpha)\dot{\gamma}_0 \left(\left| \frac{\tau^\alpha}{\tau_c^\alpha} \right| \right)^{\frac{1}{m}-1} \quad \text{(phenomenological)}$$

$$\frac{\mathrm{d}}{\mathrm{dt}}\tau_c^\alpha = \sum_\beta h_{\alpha\beta}\dot{\gamma}^\beta \quad \text{(slip resistance)}$$

$$h_{\alpha\beta} = h_0(\gamma_{acc})(q + (1-q)\delta_{\alpha\beta})$$

$$\mathbf{m}^\alpha = (\mathbf{Q}^{\mathrm{T}}\mathbf{d}_e^\alpha) \otimes (\mathbf{Q}^{\mathrm{T}}\mathbf{n}_e^\alpha)$$

$$\tau^\alpha = \boldsymbol{\Sigma}_e : \mathbf{m}^\alpha$$

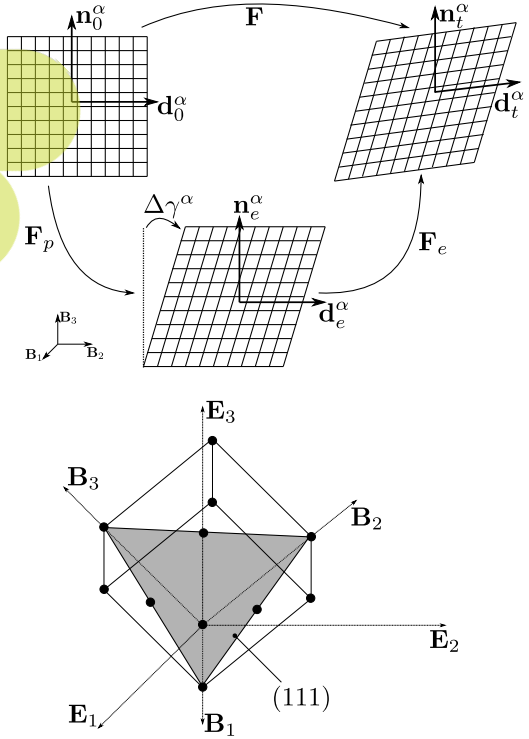

Fig. 3 Mapping of crystallographic system α by $\mathbf{F}_e$ and $\mathbf{F}_p$; Illustration of a face centered cubic unit cell with slip plane (111), rotated against global system $\{\mathbf{E}_1, \mathbf{E}_2, \mathbf{E}_3\}$

Constitutive Framework: Local and Global Update

- Local and global tangent matrices and residuals are computed by application of automation based differentiation with the software tool AceGen [5]

- Exponential map is solved via application of closed-form matrix exponential [6]

Algorithm 1: Local Routine

Given: $\mathbf{F}$, $\mathbf{F}_{p,n}, \{\tau^{\alpha}_{c,n}\}$, $\mathfrak{H}^{n}_{ip} = \mathrm{vec}\{\gamma^{\alpha}_{n}\}$
Find: $\mathbf{F}_p, \{\gamma^{\alpha}\}, \{\tau^{\alpha}_{c}\}$
initialization: $\overline{\mathfrak{H}}_{ip} \leftarrow \mathfrak{H}^{n}_{ip}$, $state \leftarrow 0$ // initial guess & set state indicator to converged state;
$\mathbf{r}_{ip} = \mathrm{vec}\{\mathbf{C}\}$;
$\{\gamma^{\alpha}\} = \overline{\mathfrak{H}}_{ip}$;
do
  compute $\mathbf{F}_p = \exp\left\{\sum_{\alpha} \Delta\gamma^{\alpha}\mathbf{m}^{\alpha}\right\}\mathbf{F}_{p,n}, \quad \mathbf{F}_e = \mathbf{F}\mathbf{F}_p^{-1}, \quad \mathbf{C}_e = \mathbf{F}_e^{\mathrm{T}}\mathbf{F}_e$;
  Set up energy density function of the lattice $\psi_{lat}(\mathbf{C}_e)$;
  compute $\mathbf{S}_e = 2\frac{\partial\psi_{lat}}{\partial\mathbf{C}_e}, \quad \boldsymbol{\Sigma}_e = \mathbf{C}_e\mathbf{S}_e, \quad \tau^{\alpha} = \boldsymbol{\Sigma}_e : \mathbf{m}^{\alpha}$;
  compute $\gamma_{acc} = \sum_{\alpha}|\Delta\gamma^{\alpha}| + \gamma_{acc,n}$, update τ^{α}_{c};
  compute $\mathcal{Q}^{k}_{ip} = \mathrm{vec}\left\{\mathrm{sign}\left(\tau^{\alpha}\right)\dot{\gamma}^{\alpha}_{0}\left(\left|\frac{\tau^{\alpha}}{\tau^{\alpha}_{c}}\right|\right)^{\frac{1}{m}-1} - \frac{\Delta\gamma^{\alpha}}{\Delta t}\right\}$;
  if $\sqrt{\mathcal{Q}^{k}_{ip}\cdot\mathcal{Q}^{k}_{ip}} < tol$ && $k == 1$ **then**
    Break // Convergence in first step of local routine. No update of history needed. Exit do-loop;
  else
    $state \leftarrow 1$ // No convergence in first step of local routine. Forcing of history update;
  end
  compute local tangent matrix $\mathcal{K}^{k}_{ip} = -\frac{\mathrm{D}\mathcal{Q}^{k}_{ip}}{\mathrm{D}\overline{\mathfrak{H}}_{ip}}$;
  obtain $\Delta\mathfrak{H}^{k+1}_{ip}$ // Through LU factorization;
  if $\sqrt{\Delta\mathfrak{H}^{k+1}_{ip}\cdot\Delta\mathfrak{H}^{k+1}_{ip}} < tol$ **then**
    compute $\mathrm{D}_{\mathbf{C}}\mathfrak{H}_{ip} = -(\mathcal{K}^{k}_{ip})^{-1}\left.\frac{\mathrm{D}\mathcal{Q}^{k}_{ip}}{\mathrm{D}\mathbf{r}_{ip}}\right|_{\overline{\mathfrak{H}}_{ip}=const.}$ evaluate sensitivity of local history field with respect to $\mathbf{C}$;
    update $\overline{\mathfrak{H}}_{ip} \leftarrow \overline{\mathfrak{H}}_{ip} + \Delta\mathfrak{H}^{k+1}_{ip}$;
    Break // Convergence in local routine reached. Exit do-loop;
  else
    update $\overline{\mathfrak{H}}_{ip} \leftarrow \overline{\mathfrak{H}}_{ip} + \Delta\mathfrak{H}^{k+1}_{ip}$;
    $k \leftarrow k+1$;
  end
while $k < maxIterNR$;
Export $\{\overline{\mathfrak{H}}_{ip}, \mathrm{D}_{\mathbf{C}}\mathfrak{H}_{ip}, state\}$;
if $state == 0$ **then**
  $\mathfrak{H}^{n+1}_{ip} \leftarrow \{\mathbf{F}_p, \mathfrak{H}^{n}_{ip}\}$ // No internal update via do-loop needed;
else
  $\{\gamma^{\alpha}\} = \overline{\mathfrak{H}}_{ip}$;
  compute $\mathbf{F}_p = \exp\left\{\sum_{\alpha}\Delta\gamma^{\alpha}\mathbf{m}^{\alpha}\right\}\mathbf{F}_{p,n}$, update γ_{acc}, τ^{α}_{c} // Force additional call of subroutine;
  $\mathfrak{H}^{n+1}_{ip} \leftarrow \overline{\mathfrak{H}}_{ip}$ // Update history field;
end
Export $\mathfrak{H}^{n+1}_{ip}$

Computational Approach: The Virtual Element Method

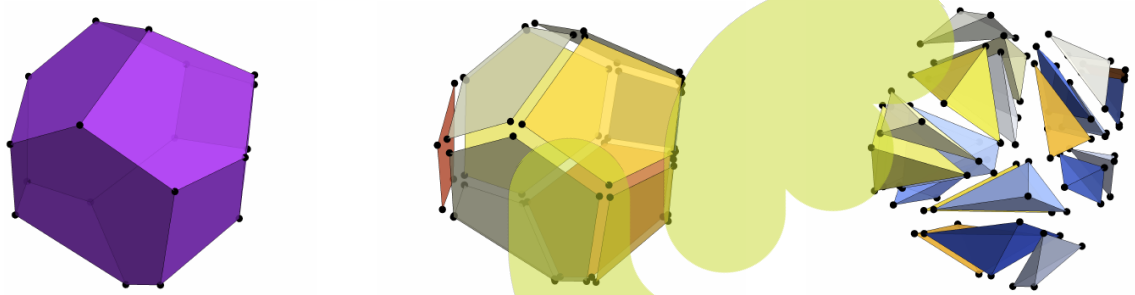

Fig. 4 A virtual element (left), its decomposition into faces (middle) and tetrahedrons (right)

Based on a split of the primary field: $\mathbf{u}_h = \Pi \mathbf{u}_h + (\mathbf{u}_h - \Pi \mathbf{u}_h)$

Projection operator Π defined such that:

$$\int_{\Omega_e} \nabla \Pi \mathbf{u}_h \mathrm{d}\Omega_e \stackrel{!}{=} \int_{\Omega_e} \nabla \mathbf{u}_h \mathrm{d}\Omega_e, \quad \frac{1}{n_v} \sum_{k=1}^{n_v} \Pi \mathbf{u}_h(\mathbf{X}) \stackrel{!}{=} \frac{1}{n_v} \sum_{k=1}^{n_v} \mathbf{u}_h(\mathbf{X})$$

Computational Approach: The Virtual Element Method

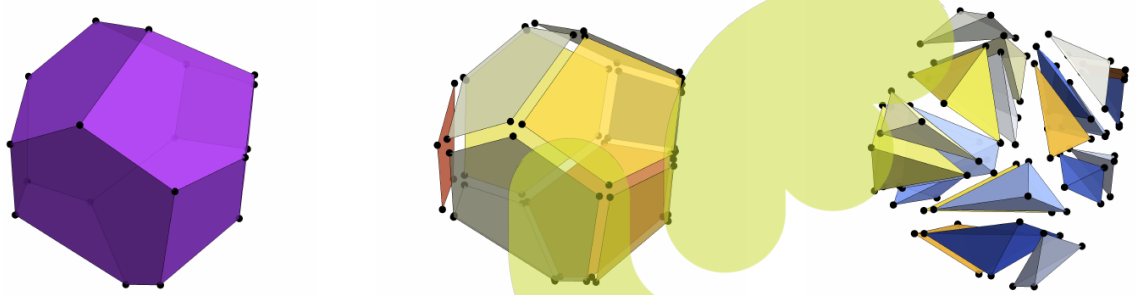

Fig. 4 A virtual element (left), its decomposition into faces (middle) and tetrahedrons (right)

Projected field is introduced by:

$\Pi \mathbf{u}_h = \sum_{i=1}^{3} (\mathbf{N}_\Pi \cdot \mathbf{a}_i)\mathbf{e}_i, \quad \mathbf{N}_\Pi = \{1, X, Y, Z\}, \quad \mathbf{a}_i = \{a_{i1}, ..., a_{i4}\}$

$\Rightarrow$ The degrees of freedom are introduced to be point-wise values at the vertices of the element

Computational Approach: The Virtual Element Method

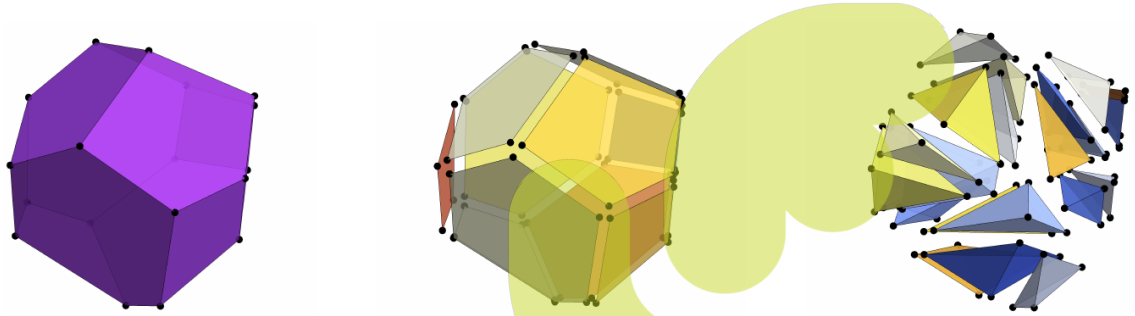

Fig. 4 A virtual element (left), its decomposition into faces (middle) and tetrahedrons (right)

$\Rightarrow$ Split of potential $U_{h,e} = (1-\beta_e)\underbrace{W_e(\nabla \mathbf{u}_h|_e)}_{\textit{consistency}} + \beta_e \underbrace{W_e(\nabla \mathbf{u}_h|_e)}_{\textit{stabilization}}$

Stabilization is computed on triangulated submesh (**Fig. 4**, right)
$\Rightarrow$ Plasticity is solved with regards to the consistency part and is shared between the subelements

Material Setup

Material data is partially taken from [3, 4]. FCC unit cell structure is considered in all numerical studies.

Table: General material input data for the numerical studies

Quantity	Description	Value
$\tau_c^\alpha(t = t_0) = \tau_0$	Initial critical resolved shear stress	14 MPa
E	Young's Modulus	$72,000$ MPa
ν	Poissons Ratio	0.33
τ_s	Saturation strength	100 MPa
m	Power-law exponent	0.02
q	Hardening-type parameter	1.4
$\dot{\gamma}_0$	Regularization rate	0.01 s^{-1}
h_0	Initial hardening modulus	5 MPa

Representative numerical examples: Evaluation of β_{min}

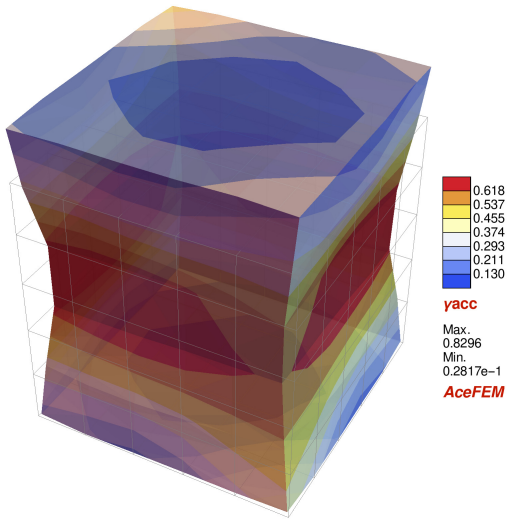

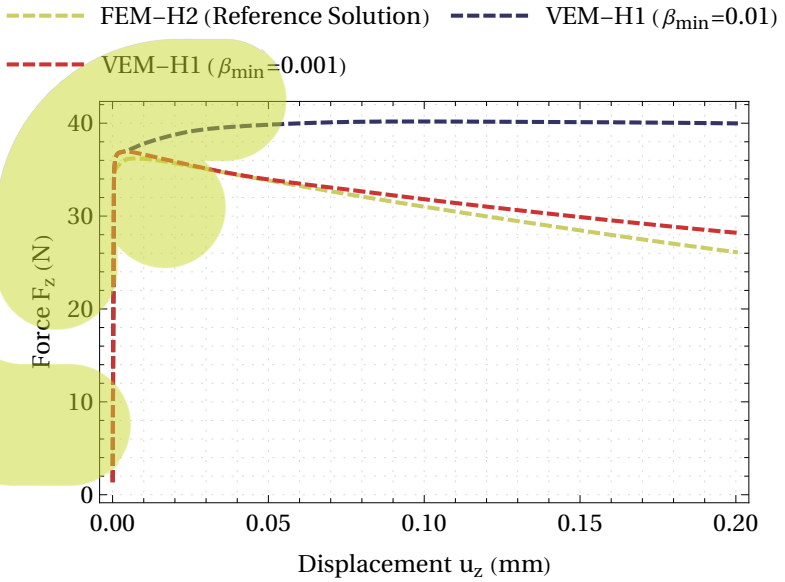

Fig. 5 Contour plot of acc. plastic shear (left) and force-displacement curves (right)

$$\beta_e = \max\{\beta_{min}, \frac{\tau_m}{E\,\gamma_{acc}}\}, \quad \tau_m = \frac{1}{n}\sum_{\alpha=1}^{n} |\tau^\alpha|$$

$\Rightarrow$ Degradation of $\beta_e \rightarrow \beta_{min}$ accounts for an overstiffening of the formulation due to plasticity (Reference FEM-H2)

Representative numerical examples: Tensile tension Test

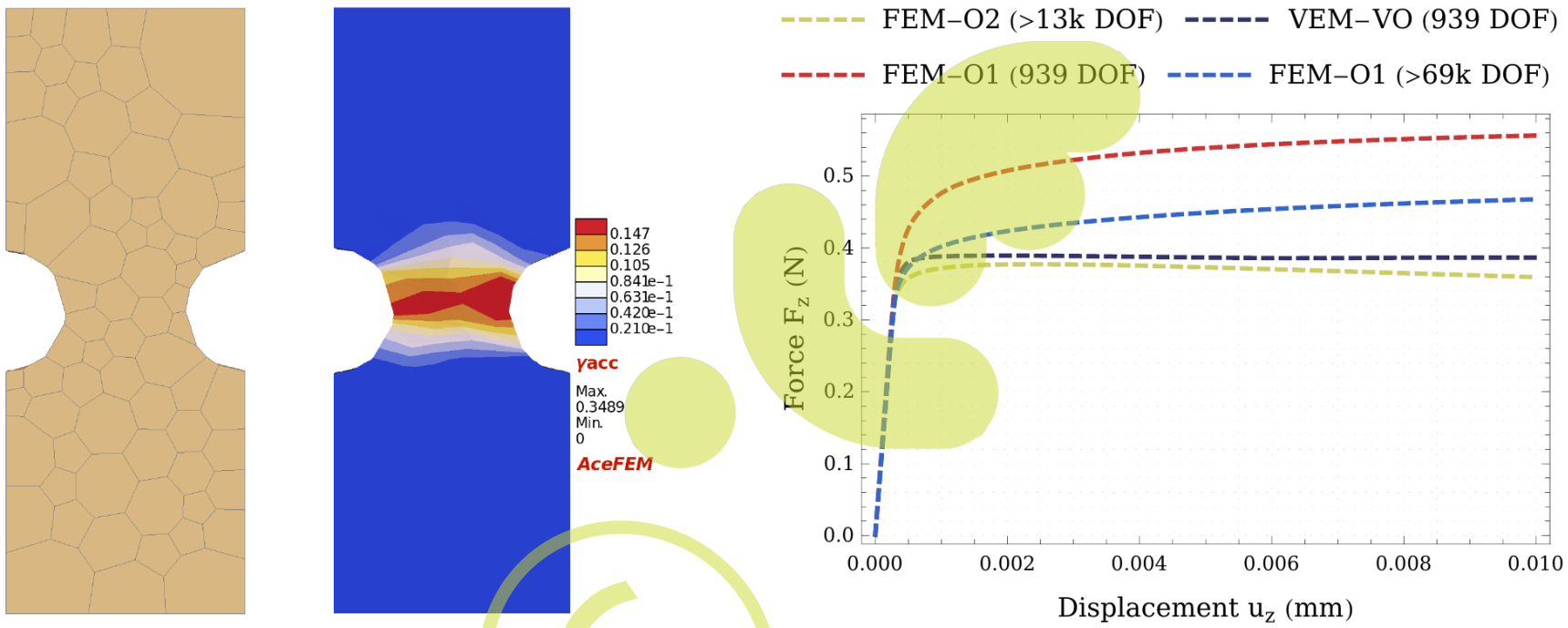

Fig. 6 Specimen (left), contour plot of acc. plastic shear, force-displacement curves for different approaches (right)

⇒ 80 virtual elements, tension in vertical direction

⇒ VEM-VO approach closely follows FM-O2 approach

Representative numerical examples: Shear Test - Setup

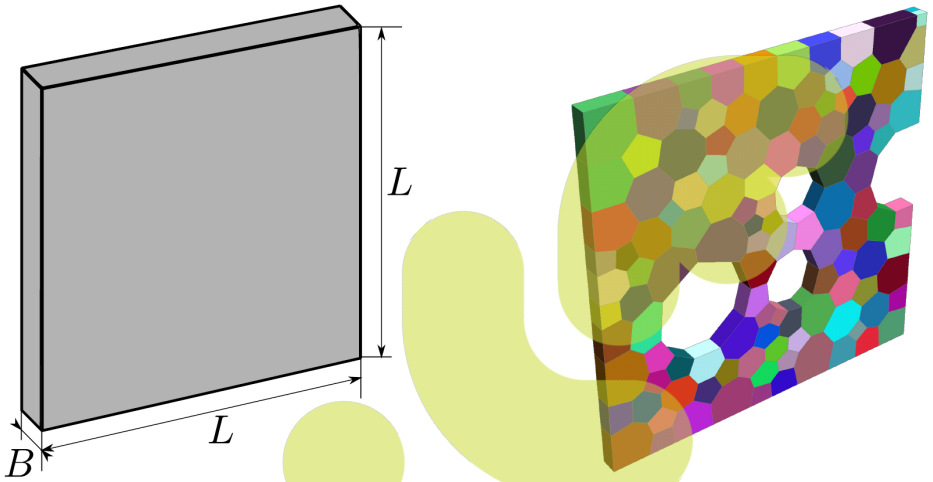

Fig. 7 Gemoetric setup (left) and plate with imperfections (right)

120 polyhedral elements

Geometric parameters: $L = 1$, $B = 1$

Deformation on boundary: $\mathbf{u}_{bc} = \bar{\mathbf{F}}\mathbf{X}_{bc} - \mathbf{X}_{bc}, \quad \bar{\mathbf{F}} = \mathbf{1} + \bar{F}_{kl}\mathbf{e}_k \otimes \mathbf{E}_l,$

$\bar{F}_{23} = \bar{F}_{32} = 0.25$

Representative numerical examples: Shear Test - Results

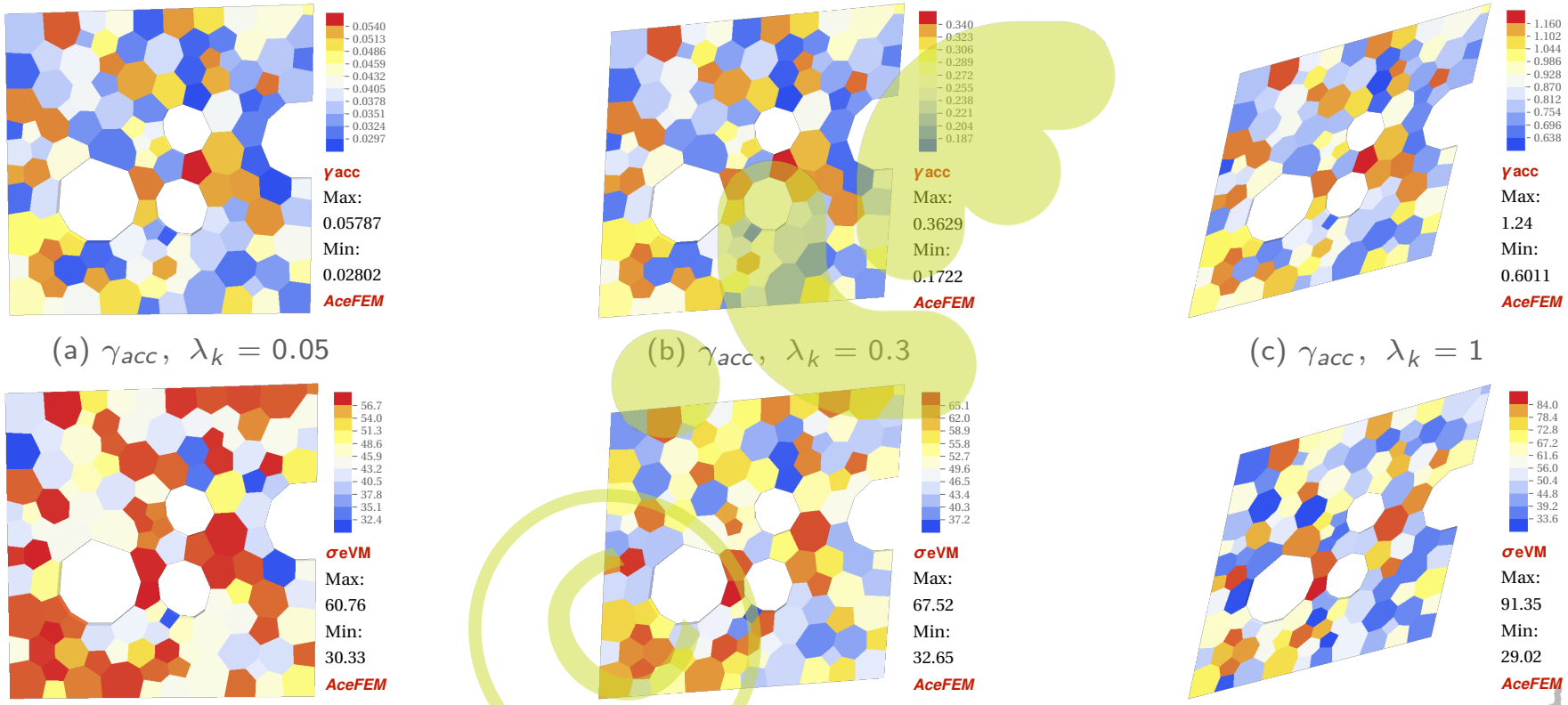

(a) γ_{acc}, $\lambda_k = 0.05$ (b) γ_{acc}, $\lambda_k = 0.3$ (c) γ_{acc}, $\lambda_k = 1$

(d) σ_{vM}, $\lambda_k = 0.05$ (e) σ_{vM}, $\lambda_k = 0.3$ (f) σ_{vM}, $\lambda_k = 1$

Fig. 8 Contour plots of acc. plastic shear (a,b,c) and *von Mises* stress (d,e,f) during deformation

Representative numerical examples: Shear Test - Maximum direction vectors

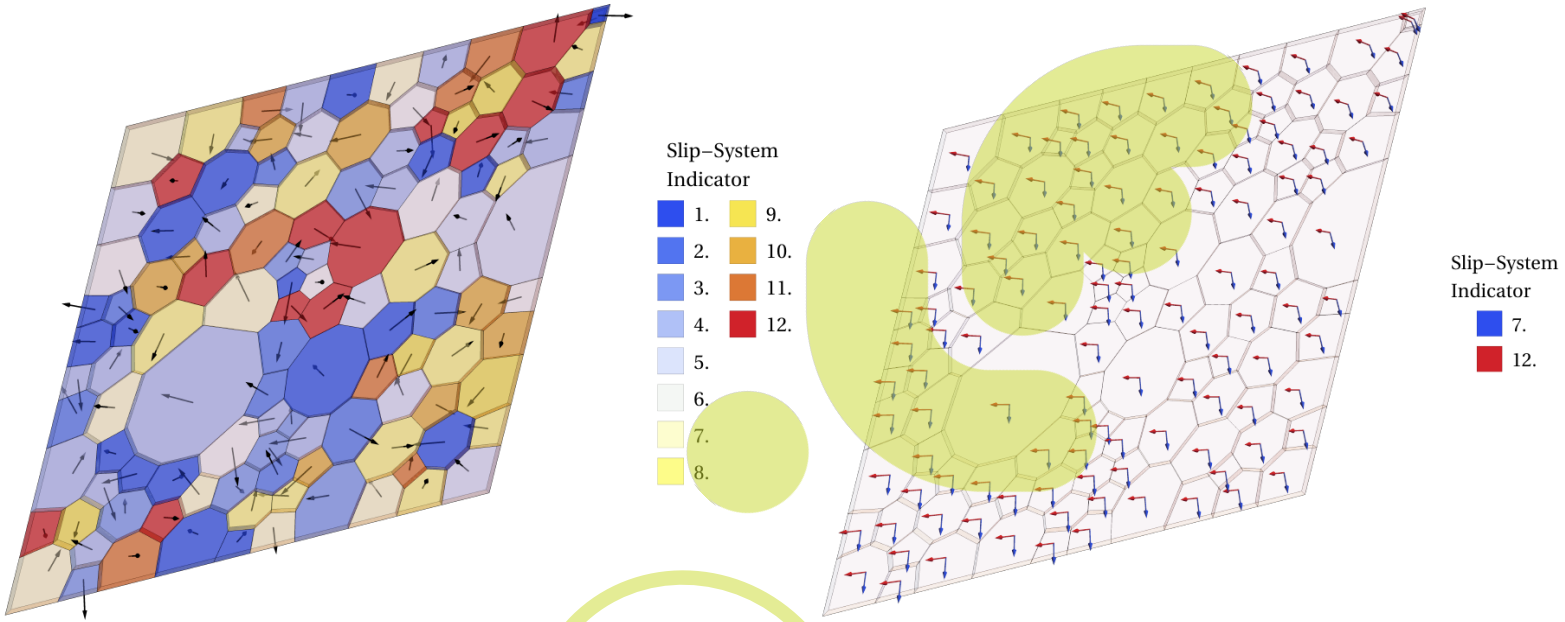

Fig. 9 Maximum direction vectors during the shear test in a polycrystalline (left) and a single crystalline setup (right)

⇒ Polycrystalline Setup - all slip systems maximal through domain

⇒ Single crystalline Setup - same slip systems in each element maximized

Representative numerical examples: 3D Grain-Assembly - Setup

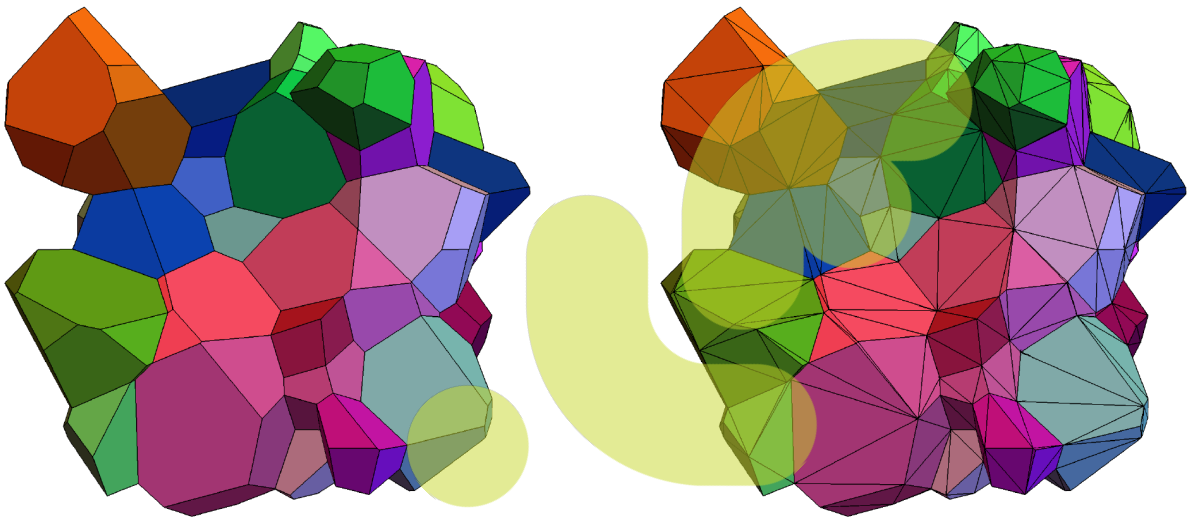

Fig. 10 Grain-Assembly. Left: meshed by VEM-VO. Right: meshed by tetrahedral elements FEM-O1

$\Rightarrow$ Homogeneous shear by $\mathbf{u}_{bc} = \bar{\mathbf{F}}\mathbf{X}_{bc} - \mathbf{X}_{bc}, \quad \bar{\mathbf{F}} = \mathbf{1} + \bar{F}_{kl}\mathbf{e}_k \otimes \mathbf{E}_l,$
$\bar{F}_{23} = \bar{F}_{32} = 0.1$

$\Rightarrow$ Computational error $\mathcal{E}_C$ evaluation

$\mathcal{E}_C = |\frac{\bar{\gamma}_{acc}(\text{Method})}{\bar{\gamma}_{acc}(\text{FEM-O2})} - 1|, \; \bar{\gamma}_{acc} = \frac{1}{V}\int_{\mathcal{B}_0} \gamma_{acc} \mathrm{d}\mathcal{B}_0$

Representative numerical examples: 3D Grain-Assembly - Results

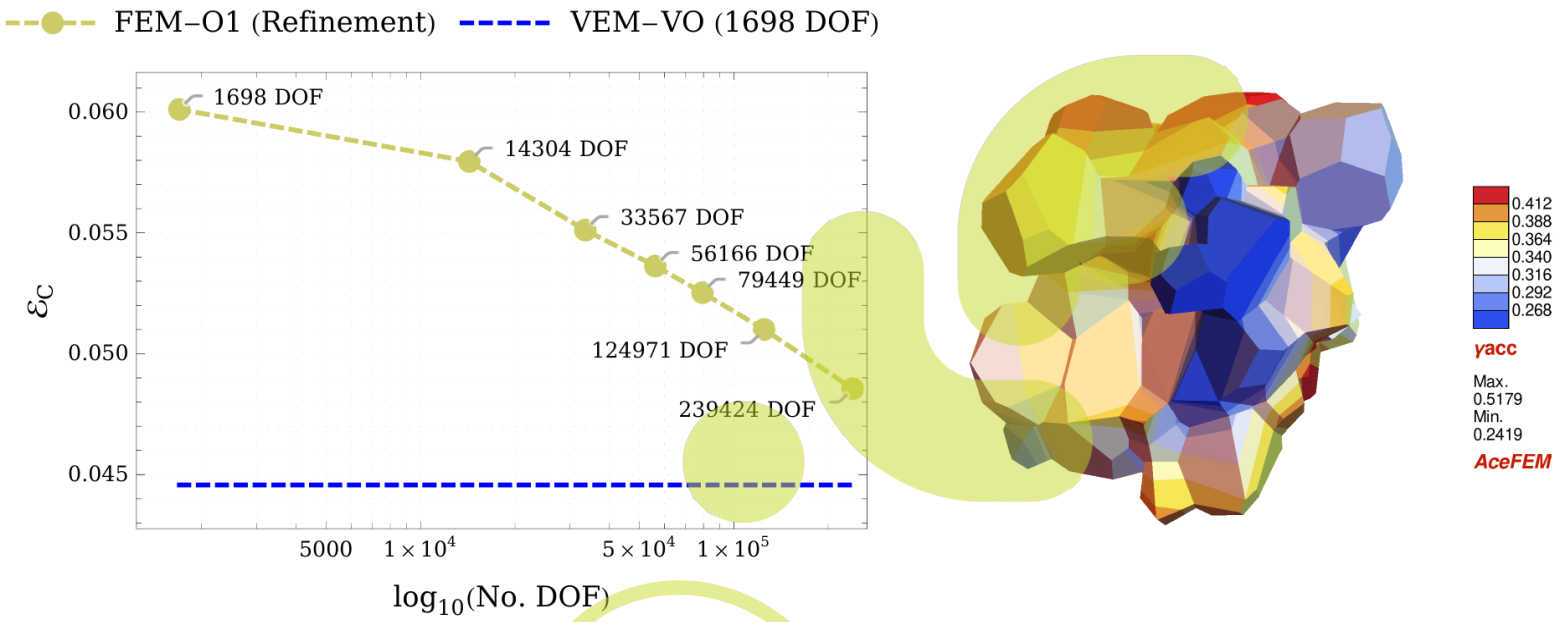

Fig. 11 Plot on computational error $\mathcal{E}_C$ (left) and contour plot of acc. plastic shear (right)

$\Rightarrow$ VEM-VO outperforms FEM-O1 approaches even at highly refined meshes (with respect to a FEM-O2 solution)

Conclusion

→ A virtual element fits perfectly heterogeneous geometries in a crystalline microstructure (VEM-VO)

→ For suitable, problem adapted, degradation of stabilization, VEM follows closely higher order FEM-O2 approaches

→ VEM-VO demonstrates higher accuracy in comparison to (even highly refined) FEM-O1 approaches

⇒ The virtual element method demonstrates a highly competetive computational approach towards efficient treatment of heterogeneous microstructures

Acknowledgement

CB, FA and PW acknowledge the financial support to this work by the German Research Foundation (DFG, Deutsche Forschungsgemeinschaft) with the collaborative research centre 1153 (SFB 1153) "Process chain for the production of hybrid high-performance components through tailored forming" with the subproject C04 "Modelling and Simulation of the Joining Zone", project number 252662854.
CB acknowledges the financial support to this presentation and to the participation at the 14th WCCM-ECCOMAS Congress by the ECCOMAS Committee in terms of the ECCOMAS scholarship.

References

[1] Herbst, S., Maier, H.J.; Nürnberger, F.: Strategies for the Heat Treatment of Steel-Aluminium Hybrid Components. *HTM Journal of Heat Treatment and Materials*, 73(5), 2018.

[2] Böhm, C., Hudobivnik, B., Marino, M., Wriggers, P.: Electro-magneto-mechanically response of polycrystalline materials: Computational Homogenization via the Virtual Element Method. *arXiv preprint arXiv:2008.01516*, 2020.

[3] Cuitino, A.M., Ortiz, M.: Computational modelling of single crystals. *Modelling and Simulation in Materials Science and Engineering*, 1(3), 225, 1993.

[4] Mlikota, M., Schmauder, S.: On the critical resolved shear stress and its importance in the fatigue performance of steel and other metals with different crystallographic structures. *Metals*, 8(11), 883, 2018.

[5] Korelc, J., Wriggers, P.: Automation of Finite Element Methods. *Springer International Publishing, Switzerland*, 2016.

[6] Korelc, J., Stupkiewicz, S.: Closed-form matrix exponential and its application in finite-strain plasticity. *International Journal for Numerical Methods in Engineering*, 98(13), 960–987, 2014.

The presentation is based on the works, presented in the contribution:
Böhm, C., Hudobivnik, B., Munk, L., Aldakheel, F., Wriggers, P.: Modelling finite deformation multi-slip scenarios at polycrystalline microstructures via the Virtual Element Method. *Under Review*, 2021.